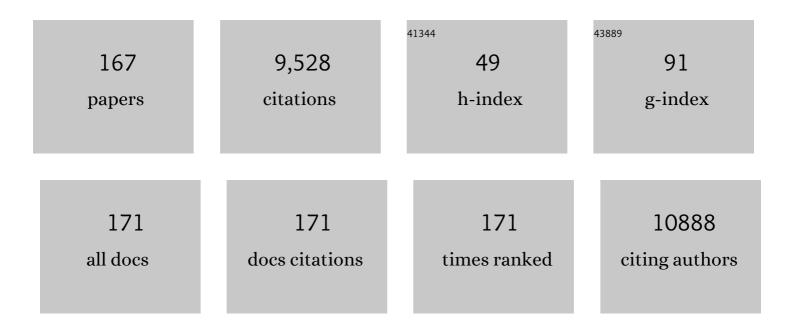
Guy Bormans

List of Publications by Year in descending order

Source: https://exaly.com/author-pdf/2555301/publications.pdf Version: 2024-02-01



CUV RODMANS

#	Article	IF	CITATIONS
1	Autologous bone marrow-derived stem-cell transfer in patients with ST-segment elevation myocardial infarction: double-blind, randomised controlled trial. Lancet, The, 2006, 367, 113-121.	13.7	1,225
2	¹⁸ Fâ€flutemetamol amyloid imaging in Alzheimer disease and mild cognitive impairment: A phase 2 trial. Annals of Neurology, 2010, 68, 319-329.	5.3	582
3	Prognostic Value of Positron Emission Tomography (PET) With Fluorine-18 Fluorodeoxyglucose ([¹⁸ F]FDC) After First-Line Chemotherapy in Non-Hodgkin's Lymphoma: Is [¹⁸ F]FDG-PET a Valid Alternative to Conventional Diagnostic Methods?. Journal of Clinical Oncology, 2001, 19, 414-419.	1.6	455
4	[18F]MK-9470, a positron emission tomography (PET) tracer for in vivo human PET brain imaging of the cannabinoid-1 receptor. Proceedings of the National Academy of Sciences of the United States of America, 2007, 104, 9800-9805.	7.1	300
5	Phase 1 Study of the Pittsburgh Compound B Derivative ¹⁸ F-Flutemetamol in Healthy Volunteers and Patients with Probable Alzheimer Disease. Journal of Nuclear Medicine, 2009, 50, 1251-1259.	5.0	273
6	Additional Value of Whole-Body Positron Emission Tomography With Fluorine-18-2-Fluoro-2-deoxy- <scp>d</scp> -glucose in Recurrent Colorectal Cancer. Journal of Clinical Oncology, 1999, 17, 894-894.	1.6	221
7	Prognostic value of pretransplantation positron emission tomography using fluorine 18-fluorodeoxyglucose in patients with aggressive lymphoma treated with high-dose chemotherapy and stem cell transplantation. Blood, 2003, 102, 53-59.	1.4	217
8	The Acyclic CB1R Inverse Agonist Taranabant Mediates Weight Loss by Increasing Energy Expenditure and Decreasing Caloric Intake. Cell Metabolism, 2008, 7, 68-78.	16.2	198
9	Impaired Myocardial Tissue Perfusion Early After Successful Thrombolysis. Circulation, 1995, 92, 2072-2078.	1.6	142
10	Characterization of pinhole SPECT acquisition geometry. IEEE Transactions on Medical Imaging, 2003, 22, 599-612.	8.9	141
11	PET Imaging of Macrophage Mannose Receptor–Expressing Macrophages in Tumor Stroma Using ¹⁸ F-Radiolabeled Camelid Single-Domain Antibody Fragments. Journal of Nuclear Medicine, 2015, 56, 1265-1271.	5.0	139
12	Attention to One or Two Features in Left or Right Visual Field: A Positron Emission Tomography Study. Journal of Neuroscience, 1997, 17, 3739-3750.	3.6	130
13	Highly Efficient Multicistronic Lentiviral Vectors with Peptide 2A Sequences. Human Gene Therapy, 2009, 20, 845-860.	2.7	128
14	Templated misfolding of Tau by prion-like seeding along neuronal connections impairs neuronal network function and associated behavioral outcomes in Tau transgenic mice. Acta Neuropathologica, 2015, 129, 875-894.	7.7	122
15	Gender-dependent increases with healthy aging of the human cerebral cannabinoid-type 1 receptor binding using [18F]MK-9470 PET. NeuroImage, 2008, 39, 1533-1541.	4.2	117
16	In Vivo Quantification of Calcitonin Gene-Related Peptide Receptor Occupancy by Telcagepant in Rhesus Monkey and Human Brain Using the Positron Emission Tomography Tracer [¹¹ C]MK-4232. Journal of Pharmacology and Experimental Therapeutics, 2013, 347, 478-486.	2.5	114
17	Widespread Decrease of Type 1 Cannabinoid Receptor Availability in Huntington Disease In Vivo. Journal of Nuclear Medicine, 2010, 51, 1413-1417.	5.0	107
18	Construction and evaluation of multitracer small-animal PET probabilistic atlases for voxel-based functional mapping of the rat brain. Journal of Nuclear Medicine, 2006, 47, 1858-66.	5.0	101

#	Article	IF	CITATIONS
19	Changes in Cerebral CB ₁ Receptor Availability after Acute and Chronic Alcohol Abuse and Monitored Abstinence. Journal of Neuroscience, 2014, 34, 2822-2831.	3.6	94
20	Increased ventral striatal CB1 receptor binding is related to negative symptoms in drug-free patients with schizophrenia. NeuroImage, 2013, 79, 304-312.	4.2	93
21	Brain Imaging of Alzheimer Dementia Patients and Elderly Controls with ¹⁸ F-MK-6240, a PET Tracer Targeting Neurofibrillary Tangles. Journal of Nuclear Medicine, 2019, 60, 107-114.	5.0	92
22	Synthesis and Evaluation of ¹⁸ F-Labeled 2-Phenylbenzothiazoles as Positron Emission Tomography Imaging Agents for Amyloid Plaques in Alzheimer's Disease. Journal of Medicinal Chemistry, 2009, 52, 1428-1437.	6.4	87
23	Positron emission tomography, magnetic resonance imaging and proton NMR spectroscopy of white matter in multiple sclerosis. Multiple Sclerosis Journal, 1997, 3, 8-17.	3.0	86
24	Necrosis Avid Contrast Agents. Investigative Radiology, 2005, 40, 526-535.	6.2	82
25	A Dual-targeting Anticancer Approach: Soil and Seed Principle. Radiology, 2011, 260, 799-807.	7.3	81
26	Brain Type 1 Cannabinoid Receptor Availability in Patients with Anorexia and Bulimia Nervosa. Biological Psychiatry, 2011, 70, 777-784.	1.3	78
27	Preclinical Evaluation of a P2X7 Receptor–Selective Radiotracer: PET Studies in a Rat Model with Local Overexpression of the Human P2X7 Receptor and in Nonhuman Primates. Journal of Nuclear Medicine, 2016, 57, 1436-1441.	5.0	77
28	Design and Challenges of Radiopharmaceuticals. Seminars in Nuclear Medicine, 2019, 49, 339-356.	4.6	76
29	Longitudinal follow-up and characterization of a robust rat model for Parkinson's disease based on overexpression of alpha-synuclein with adeno-associated viral vectors. Neurobiology of Aging, 2015, 36, 1543-1558.	3.1	75
30	Preclinical Evaluation of ¹⁸ F-JNJ64349311, a Novel PET Tracer for Tau Imaging. Journal of Nuclear Medicine, 2017, 58, 975-981.	5.0	72
31	Non-invasive detection and quantification of acute myocardial infarction in rabbits using mono-[1231]iodohypericin ÂSPECT. European Heart Journal, 2007, 29, 260-269.	2.2	68
32	Mammalian models of chemically induced primary malignancies exploitable for imaging-based preclinical theragnostic research. Quantitative Imaging in Medicine and Surgery, 2015, 5, 708-29.	2.0	67
33	Visualisation of loss of 5-HT2A receptors with age in healthy volunteers using [18F]altanserin and positron emission tomographic imaging. Psychiatry Research - Neuroimaging, 1996, 68, 11-22.	1.8	65
34	Preclinical Evaluation of ¹⁸ F-JNJ41510417 as a Radioligand for PET Imaging of Phosphodiesterase-10A in the Brain. Journal of Nuclear Medicine, 2010, 51, 1584-1591.	5.0	64
35	AÂ amyloid deposition in the language system and how the brain responds. Brain, 2007, 130, 2055-2069.	7.6	63
36	De novo design of a biologically active amyloid. Science, 2016, 354, .	12.6	63

#	Article	lF	CITATIONS
37	¹⁸ F-JNJ-64413739, a Novel PET Ligand for the P2X7 Ion Channel: Radiation Dosimetry, Kinetic Modeling, Test-Retest Variability, and Occupancy of the P2X7 Antagonist JNJ-54175446. Journal of Nuclear Medicine, 2019, 60, 683-690.	5.0	63
38	Optimization of geometrical calibration in pinhole SPECT. IEEE Transactions on Medical Imaging, 2005, 24, 180-190.	8.9	61
39	Noninvasive Monitoring of Long-Term Lentiviral Vector-Mediated Gene Expression in Rodent Brain with Bioluminescence Imaging. Molecular Therapy, 2006, 14, 423-431.	8.2	60
40	¹⁸ F-FDG Labeling of Mesenchymal Stem Cells and Multipotent Adult Progenitor Cells for PET Imaging: Effects on Ultrastructure and Differentiation Capacity. Journal of Nuclear Medicine, 2013, 54, 447-454.	5.0	60
41	Development of Superparamagnetic Nanoparticles Coated with Polyacrylic Acid and Aluminum Hydroxide as an Efficient Contrast Agent for Multimodal Imaging. Nanomaterials, 2019, 9, 1626.	4.1	59
42	[18F]AlF-NOTA-octreotide PET imaging: biodistribution, dosimetry and first comparison with [68Ca]Ga-DOTATATE in neuroendocrine tumour patients. European Journal of Nuclear Medicine and Molecular Imaging, 2020, 47, 3033-3046.	6.4	59
43	Scintigraphic evaluation in rabbits of nasal drug delivery systems based on carbopol 971p® and carboxymethylcellulose. Journal of Controlled Release, 2000, 68, 207-214.	9.9	57
44	Human Brain Activity Related to Orientation Discrimination Tasks. European Journal of Neuroscience, 1997, 9, 246-259.	2.6	55
45	Optimal buffer choice of the radiosynthesis of 68Ga–Dotatoc for clinical application. Nuclear Medicine Communications, 2010, 31, 753-758.	1.1	55
46	[11C]JNJ54173717, a novel P2X7 receptor radioligand as marker for neuroinflammation: human biodistribution, dosimetry, brain kinetic modelling and quantification of brain P2X7 receptors in patients with Parkinson's disease and healthy volunteers. European Journal of Nuclear Medicine and Molecular Imaging, 2019, 46, 2051-2064.	6.4	55
47	Somatostatin receptor PET ligands - the next generation for clinical practice. American Journal of Nuclear Medicine and Molecular Imaging, 2018, 8, 311-331.	1.0	55
48	Al ¹⁸ F-Labeling Of Heat-Sensitive Biomolecules for Positron Emission Tomography Imaging. Theranostics, 2017, 7, 2924-2939.	10.0	54
49	Measuring extrastriatal dopamine release during a reward learning task. Human Brain Mapping, 2013, 34, 575-586.	3.6	51
50	In vivo type 1 cannabinoid receptor availability in Alzheimer's disease. European Neuropsychopharmacology, 2014, 24, 242-250.	0.7	51
51	Optimized In Vivo Detection of Dopamine Release Using ¹⁸ F-Fallypride PET. Journal of Nuclear Medicine, 2012, 53, 1565-1572.	5.0	49
52	In vitro evaluation and biodistribution of a 99mTc-labeled anti-VEGF peptide targeting neuropilin-1. Nuclear Medicine and Biology, 2004, 31, 575-581.	0.6	48
53	Synthesis, Evaluation, and Radiolabeling of New Potent Positive Allosteric Modulators of the Metabotropic Glutamate Receptor 2 as Potential Tracers for Positron Emission Tomography Imaging. Journal of Medicinal Chemistry, 2012, 55, 8685-8699.	6.4	48
54	PET imaging of TSPO in a rat model of local neuroinflammation induced by intracerebral injection of lipopolysaccharide. Nuclear Medicine and Biology, 2015, 42, 753-761.	0.6	48

#	Article	IF	CITATIONS
55	Guidelines for the content and format of PET brain data in publications and archives: A consensus paper. Journal of Cerebral Blood Flow and Metabolism, 2020, 40, 1576-1585.	4.3	47
56	Retention of [18F]fluoride on reversed phase HPLC columns. Journal of Pharmaceutical and Biomedical Analysis, 2015, 111, 209-214.	2.8	46
57	Non-invasive imaging of neuropathology in a rat model of α-synuclein overexpression. Neurobiology of Aging, 2007, 28, 248-257.	3.1	45
58	Increased Cerebral Cannabinoid-1 Receptor Availability Is a Stable Feature of Functional Dyspepsia: A [18F]MK-9470 PET Study. Psychotherapy and Psychosomatics, 2015, 84, 149-158.	8.8	45
59	Bismuth-213 for Targeted Radionuclide Therapy: From Atom to Bedside. Pharmaceutics, 2021, 13, 599.	4.5	45
60	A PET Brain Reporter Gene System Based on Type 2 Cannabinoid Receptors. Journal of Nuclear Medicine, 2011, 52, 1102-1109.	5.0	44
61	Synthesis and Evaluation of ¹⁸ F- and ¹¹ C-Labeled Phenyl-Galactopyranosides as Potential Probes for <i>in Vivo</i> Visualization of LacZ Gene Expression using Positron Emission Tomography. Bioconjugate Chemistry, 2008, 19, 441-449.	3.6	43
62	Synthesis, In Vivo Occupancy, and Radiolabeling of Potent Phosphodiesterase Subtype-10 Inhibitors as Candidates for Positron Emission Tomography Imaging. Journal of Medicinal Chemistry, 2011, 54, 5820-5835.	6.4	43
63	Quantification of ¹⁸ F-JNJ-42259152, a Novel Phosphodiesterase 10A PET Tracer: Kinetic Modeling and Test–Retest Study in Human Brain. Journal of Nuclear Medicine, 2013, 54, 1285-1293.	5.0	43
64	On the consensus nomenclature rules for radiopharmaceutical chemistry – Reconsideration of radiochemical conversion. Nuclear Medicine and Biology, 2021, 93, 19-21.	0.6	43
65	Motor- and food-related metabolic cerebral changes in the activity-based rat model for anorexia nervosa: A voxel-based microPET study. NeuroImage, 2007, 35, 214-221.	4.2	42
66	Radiolabeled iodohypericin as tumor necrosis avid tracer: diagnostic and therapeutic potential. International Journal of Cancer, 2012, 131, E129-37.	5.1	42
67	TSPO Versus P2X7 as a Target for Neuroinflammation: An In Vitro and In Vivo Study. Journal of Nuclear Medicine, 2020, 61, 604-607.	5.0	42
68	PET Radioligands for In Vivo Visualization of Neuroinflammation. Current Pharmaceutical Design, 2014, 20, 5897-5913.	1.9	42
69	The Presence of Ethanol in Radiopharmaceutical Injections. Journal of Nuclear Medicine, 2008, 49, 2071-2071.	5.0	39
70	Preliminary in vivo evaluation of a novel 99mTc-Labeled HYNIC-cys-annexin A5 as an apoptosis imaging agent. Bioorganic and Medicinal Chemistry Letters, 2008, 18, 3794-3798.	2.2	38
71	Whole-Body Biodistribution and Radiation Dosimetry of the Human Cannabinoid Type-1 Receptor Ligand ¹⁸ F-MK-9470 in Healthy Subjects. Journal of Nuclear Medicine, 2008, 49, 439-445.	5.0	38
72	In vivo type 1 cannabinoid receptor mapping in the 6-hydroxydopamine lesion rat model of Parkinson's disease. Brain Research, 2010, 1316, 153-162.	2.2	38

#	Article	IF	CITATIONS
73	Pretargeted PET Imaging Using a Bioorthogonal ¹⁸ F-Labeled <i>trans</i> -Cyclooctene in an Ovarian Carcinoma Model. Bioconjugate Chemistry, 2017, 28, 2915-2920.	3.6	38
74	Development of a Conjugate of99mTc-EC with Aminomethylenediphosphonate in the Search for a Bone Tracer with Fast Clearance from Soft Tissue. Bioconjugate Chemistry, 2002, 13, 16-22.	3.6	37
75	Comparison of New Tau PET-Tracer Candidates With [¹⁸ F]T808 and [¹⁸ F]T807. Molecular Imaging, 2016, 15, 153601211562492.	1.4	37
76	Micro-flow photosynthesis of new dienophiles for inverse-electron-demand Diels–Alder reactions. Potential applications for pretargeted in vivo PET imaging. Chemical Science, 2017, 8, 1251-1258.	7.4	37
77	Regions in the human brain activated by simultaneous orientation discrimination: a study with positron emission tomography. European Journal of Neuroscience, 1998, 10, 3689-3699.	2.6	34
78	An in vivo [18F]MK-9470 microPET study of type 1 cannabinoid receptor binding in Wistar rats after chronic administration of valproate and levetiracetam. Neuropharmacology, 2008, 54, 1103-1106.	4.1	34
79	Regional brain activity during shape recognition impaired by a scopolamine challenge to encoding. European Journal of Neuroscience, 1999, 11, 3701-3714.	2.6	33
80	Synthesis and evaluation of a 99mTc-MAMA-propyl-thymidine complex as a potential probe for in vivo visualization of tumor cell proliferation with SPECT. Nuclear Medicine and Biology, 2007, 34, 283-291.	0.6	33
81	Early decrease of type 1 cannabinoid receptor binding and phosphodiesterase 10A activity inÂvivo in R6/2 Huntington mice. Neurobiology of Aging, 2014, 35, 2858-2869.	3.1	32
82	Development and Evaluation of Interleukin-2–Derived Radiotracers for PET Imaging of T Cells in Mice. Journal of Nuclear Medicine, 2020, 61, 1355-1360.	5.0	32
83	What We Observe In Vivo Is Not Always What We See In Vitro: Development and Validation of 11C-JNJ-42491293, A Novel Radioligand for mGluR2. Journal of Nuclear Medicine, 2017, 58, 110-116.	5.0	31
84	Recent Progress in Metal Catalyzed Direct Carboxylation of Aryl Halides and Pseudo Halides Employing CO ₂ : Opportunities for ¹¹ Câ€Radiochemistry. ChemCatChem, 2016, 8, 3692-3700.	3.7	30
85	Cerebral dopaminergic and glutamatergic transmission relate to different subjective responses of acute alcohol intake: an in vivo multimodal imaging study. Addiction Biology, 2018, 23, 931-944.	2.6	30
86	Al18F-NOTA-octreotide: first comparison with 68Ga-DOTATATE in a neuroendocrine tumour patient. European Journal of Nuclear Medicine and Molecular Imaging, 2019, 46, 2398-2399.	6.4	30
87	Identity confirmation of 99mTc-MAG3, 99mTc-Sestamibi and 99mTc-ECD using radio-LC-MS. Journal of Pharmaceutical and Biomedical Analysis, 2003, 32, 669-678.	2.8	29
88	Guidelines to PET measurements of the target occupancy in the brain for drug development. European Journal of Nuclear Medicine and Molecular Imaging, 2016, 43, 2255-2262.	6.4	28
89	Simultaneous in vivo PET/MRI using fluorine-18 labeled Fe3O4@Al(OH)3 nanoparticles: comparison of nanoparticle and nanoparticle-labeled stem cell distribution. EJNMMI Research, 2020, 10, 73.	2.5	28
90	cGMP production of the radiopharmaceutical [¹⁸ F]MK-6240 for PET imaging of human neurofibrillary tangles. Journal of Labelled Compounds and Radiopharmaceuticals, 2017, 60, 263-269.	1.0	27

#	Article	IF	CITATIONS
91	Lower Limbic Metabotropic Glutamate Receptor 5 Availability in Alcohol Dependence. Journal of Nuclear Medicine, 2018, 59, 682-690.	5.0	27
92	Direct fluorine-18 labeling of heat-sensitive biomolecules for positron emission tomography imaging using the Al18F-RESCA method. Nature Protocols, 2018, 13, 2330-2347.	12.0	27
93	Preclinical evaluation of [¹⁸ F]MA3: a CB ₂ receptor agonist radiotracer for PET. British Journal of Pharmacology, 2019, 176, 1481-1491.	5.4	26
94	Translation of HDAC6 PET Imaging Using [¹⁸ F]EKZ-001–cGMP Production and Measurement of HDAC6 Target Occupancy in Nonhuman Primates. ACS Chemical Neuroscience, 2020, 11, 1093-1101.	3.5	26
95	Regional myocardial blood flow, glucose utilization and contractile function before and after revascularization and ultrastructural findings in patients with chronic coronary artery disease. European Journal of Nuclear Medicine and Molecular Imaging, 1995, 22, 1299-1305.	2.1	25
96	Influence of Chronic Nicotine Administration on Cerebral Type 1 Cannabinoid Receptor Binding: An In Vivo Micro-PET Study in the Rat Using [18F]MK-9470. Journal of Molecular Neuroscience, 2010, 42, 162-167.	2.3	25
97	Development and evaluation of a 68Ga labeled pamoic acid derivative for in vivo visualization of necrosis using positron emission tomography. Bioorganic and Medicinal Chemistry, 2010, 18, 5274-5281.	3.0	25
98	Interictal Type 1 Cannabinoid Receptor Binding is Increased in Female Migraine Patients. Headache, 2012, 52, 433-440.	3.9	25
99	Reverse engineering synthetic antiviral amyloids. Nature Communications, 2020, 11, 2832.	12.8	25
100	Necrosis Avidity of ^{99m} Tc(CO) ₃ -Labeled Pamoic acid Derivatives: Synthesis and Preliminary Biological Evaluation in Animal Models of Necrosis. Bioconjugate Chemistry, 2007, 18, 1924-1934.	3.6	24
101	Synthesis and preliminary evaluation of mono-[123I]iodohypericin monocarboxylic acid as a necrosis avid imaging agent. Bioorganic and Medicinal Chemistry Letters, 2007, 17, 4001-4005.	2.2	24
102	Evaluation of [18F]MK-0911, a positron emission tomography (PET) tracer for opioid receptor-like 1 (ORL1), in rhesus monkey and human. NeuroImage, 2013, 68, 1-10.	4.2	24
103	Discovery of <i>N</i> -(4-[¹⁸ F]Fluoro-5-methylpyridin-2-yl)isoquinolin-6-amine (JNJ-64326067), a New Promising Tau Positron Emission Tomography Imaging Tracer. Journal of Medicinal Chemistry, 2019, 62, 2974-2987.	6.4	24
104	Recovery of Decreased Metabotropic Glutamate Receptor 5 Availability in Abstinent Alcohol-Dependent Patients. Journal of Nuclear Medicine, 2020, 61, 256-262.	5.0	24
105	Evaluation of tumor affinity of mono-[123I]iodohypericin and mono-[123I]iodoprotohypericin in a mouse model with a RIF-1 tumor. Contrast Media and Molecular Imaging, 2007, 2, 113-119.	0.8	23
106	In Vivo Characterization and Dynamic Receptor Occupancy Imaging of TPA023B, an α2/α3/α5 Subtype Selective γ-Aminobutyric Acid–A Partial Agonist. Biological Psychiatry, 2008, 64, 153-161.	1.3	23
107	11C-MK-8278 PET as a Tool for Pharmacodynamic Brain Occupancy of Histamine 3 Receptor Inverse Agonists. Journal of Nuclear Medicine, 2014, 55, 65-72.	5.0	23
108	Synthesis and preclinical evaluation of [11 C]MA-PB-1 for inÂvivo imaging of brain monoacylglycerol lipase (MAGL). European Journal of Medicinal Chemistry, 2017, 136, 104-113.	5.5	23

#	Article	IF	CITATIONS
109	Drug Development in Alzheimer's Disease: The Contribution of PET and SPECT. Frontiers in Pharmacology, 2016, 7, 88.	3.5	22
110	Cholinergic depletion and basal forebrain volume in primary progressive aphasia. Neurolmage: Clinical, 2017, 13, 271-279.	2.7	22
111	Preclinical Evaluation and Quantification of ¹⁸ F-FPEB as a Radioligand for PET Imaging of the Metabotropic Glutamate Receptor 5. Journal of Nuclear Medicine, 2015, 56, 1954-1959.	5.0	21
112	Preclinical Safety Evaluation and Human Dosimetry of [18F]MK-6240, a Novel PET Tracer for Imaging Neurofibrillary Tangles. Molecular Imaging and Biology, 2020, 22, 173-180.	2.6	21
113	Positive Association Between Limbic Metabotropic Glutamate Receptor 5 Availability and Novelty-Seeking Temperament in Humans: An ¹⁸ F-FPEB PET Study. Journal of Nuclear Medicine, 2016, 57, 1746-1752.	5.0	20
114	Accumulation and Photocytotoxicity of Hypericin and Analogs in Two- and Three-Dimensional Cultures of Transitional Cell Carcinoma Cells¶. Photochemistry and Photobiology, 2003, 78, 607.	2.5	18
115	Improved synthesis and metabolic stability analysis of the dopamine transporter ligand [18F]FECT. Nuclear Medicine and Biology, 2008, 35, 75-82.	0.6	18
116	Recent Advances in Positron Emission Tomography (PET) Radiotracers for Imaging Phosphodiesterases. Current Topics in Medicinal Chemistry, 2012, 12, 1224-1236.	2.1	18
117	Kinetic modeling and longâ€ŧerm testâ€ŧetest reproducibility of the mGluR5 PET tracer ¹⁸ Fâ€FPEB in human brain. Synapse, 2016, 70, 153-162.	1.2	18
118	Glutamatergic Biomarkers for Cocaine Addiction: A Longitudinal Study Using MR Spectroscopy and mGluR5 PET in Self-Administering Rats. Journal of Nuclear Medicine, 2018, 59, 952-959.	5.0	18
119	Effect of corticosteroids on 18F-FDG uptake in tumor lesions after chemotherapy. Journal of Nuclear Medicine, 2007, 48, 390-7.	5.0	18
120	Characterization of the novel GlyT1 PET tracer [¹⁸ F]MKâ€6577 in humans. Synapse, 2015, 69, 33-40.	1.2	17
121	The first study on therapeutic efficacies of a vascular disrupting agent CA4P among primary hepatocellular carcinomas with a full spectrum of differentiation and vascularity: Correlation of MRIâ€microangiographyâ€histopathology in rats. International Journal of Cancer, 2018, 143, 1817-1828.	5.1	17
122	Effects of alcohol exposure on the glutamatergic system: a combined longitudinal ¹⁸ Fâ€FPEB and ¹ Hâ€MRS study in rats. Addiction Biology, 2019, 24, 696-706.	2.6	17
123	Improved resolution and sensitivity of [18F]MFBG PET compared with [123I]MIBG SPECT in a patient with a norepinephrine transporter–expressing tumour. European Journal of Nuclear Medicine and Molecular Imaging, 2021, 48, 313-315.	6.4	17
124	Synthesis and Evaluation of Three ¹⁸ F-Labeled Aminophenylbenzothiazoles as Amyloid Imaging Agents. Journal of Medicinal Chemistry, 2009, 52, 7090-7102.	6.4	16
125	Evaluation of PET radioligands for in vivo visualization of phosphodiesterase 5 (PDE5). Nuclear Medicine and Biology, 2014, 41, 155-162.	0.6	16
126	Clinical validation of the novel HDAC6 radiotracer [18F]EKZ-001 in the human brain. European Journal of Nuclear Medicine and Molecular Imaging, 2021, 48, 596-611.	6.4	16

#	Article	IF	CITATIONS
127	Construction and Evaluation of Quantitative Small-Animal PET Probabilistic Atlases for [18F]FDG and [18F]FECT Functional Mapping of the Mouse Brain. PLoS ONE, 2013, 8, e65286.	2.5	16
128	Synthesis of [18F]RGD-K5 by catalyzed [3+2] cycloaddition for imaging integrin αvβ3 expression in vivo. Nuclear Medicine and Biology, 2013, 40, 710-716.	0.6	15
129	Synthesis and biological evaluation of carbon-11 and fluorine-18 labeled tracers for in vivo visualization of PDE10A. Nuclear Medicine and Biology, 2014, 41, 695-704.	0.6	15
130	PET reversed mismatch in an experimental model of subacute myocardial infarction. European Journal of Nuclear Medicine and Molecular Imaging, 2001, 28, 457-465.	2.1	14
131	Pretargeting of necrotic tumors with biotinylated hypericin using 1231-labeled avidin: evaluation of a two-step strategy. Investigational New Drugs, 2012, 30, 2132-2140.	2.6	14
132	[18F] <scp>JNJ</scp> 42259152 binding to phosphodiesterase 10A, a key regulator of medium spiny neuron excitability, is altered in the presence of cyclic <scp>AMP</scp> . Journal of Neurochemistry, 2016, 139, 897-906.	3.9	14
133	Influence of chronic bromocriptine and levodopa administration on cerebral type 1 cannabinoid receptor binding. Synapse, 2010, 64, 617-623.	1.2	13
134	Synthesis and biological evaluation of [11C]SB366791: A new PET-radioligand for in vivo imaging of the TRPV1 receptor. Nuclear Medicine and Biology, 2013, 40, 141-147.	0.6	13
135	Synthesis and biological evaluation of 11C-labeled β-galactosyl triazoles as potential PET tracers for in vivo LacZ reporter gene imaging. Bioorganic and Medicinal Chemistry, 2009, 17, 5117-5125.	3.0	12
136	New Transient Receptor Potential Vanilloid Subfamily Member 1 Positron Emission Tomography Radioligands: Synthesis, Radiolabeling, and Preclinical Evaluation. ACS Chemical Neuroscience, 2013, 4, 624-634.	3.5	12
137	Development and biological evaluation of 99mTc-BAT-tropane esters. Nuclear Medicine and Biology, 2005, 32, 607-612.	0.6	11
138	Evaluation of [¹¹ C]NMS-E973 as a PET tracer for <i>in vivo</i> visualisation of HSP90. Theranostics, 2019, 9, 554-572.	10.0	11
139	Predicting Therapeutic Efficacy of Vascular Disrupting Agent CA4P in Rats with Liver Tumors by Hepatobiliary Contrast Agent Mn-DPDP-Enhanced MRI. Translational Oncology, 2020, 13, 92-101.	3.7	11
140	Evaluation of [11C]KB631 as a PET tracer for in vivo visualisation of HDAC6 in B16.F10 melanoma. Nuclear Medicine and Biology, 2019, 74-75, 1-11.	0.6	10
141	The PET tracer [¹¹ C]MK-6884 quantifies M4 muscarinic receptor in rhesus monkeys and patients with Alzheimer's disease. Science Translational Medicine, 2022, 14, eabg3684.	12.4	10
142	Structure-Based Design, Optimization, and Development of [¹⁸ F]LU13: A Novel Radioligand for Cannabinoid Receptor Type 2 Imaging in the Brain with PET. Journal of Medicinal Chemistry, 2022, 65, 9034-9049.	6.4	10
143	Radiolabeling and preliminary biological evaluation of a 99mTc(CO)3 labeled 3,3′-(benzylidene)-bis-(1H-indole-2-carbohydrazide) derivative as a potential SPECT tracer for in vivo visualization of necrosis. Bioorganic and Medicinal Chemistry Letters, 2011, 21, 502-505.	2.2	9
144	Brain PET imaging of phosphodiesterase 10A in progressive supranuclear palsy and Parkinson's disease. Movement Disorders, 2017, 32, 943-945.	3.9	9

#	Article	IF	CITATIONS
145	The Effect of a Methyl or 2-fluoroethyl Substituent at the N-3 Position of Thymidine, 3′-fluoro-3′-deoxythymi-dine and 1-β-D-arabinosylthymine on Their Antiviral and Cytostatic Activity in Cell Culture. Antiviral Chemistry and Chemotherapy, 2006, 17, 17-23.	0.6	8
146	Synthesis and biological evaluation of 68Ga labeled bis-DOTA-3,3′-(benzylidene)-bis-(1H-indole-2-carbohydrazide) as a PET tracer for in vivo visualization of necrosis. Bioorganic and Medicinal Chemistry Letters, 2013, 23, 3216-3220.	2.2	8
147	Carbon-11 and Fluorine-18 Radiolabeled Pyridopyrazinone Derivatives for Positron Emission Tomography (PET) Imaging of Phosphodiesterase-5 (PDE5). Journal of Medicinal Chemistry, 2017, 60, 486-496.	6.4	8
148	Radiolabeling of Human Serum Albumin With Terbium-161 Using Mild Conditions and Evaluation of in vivo Stability. Frontiers in Medicine, 2021, 8, 675122.	2.6	8
149	Characterisation and biodistribution of two neutral 99mTc(CO)3 complexes with a tridentate ligand. Bioorganic and Medicinal Chemistry Letters, 2005, 15, 4192-4195.	2.2	7
150	99mTc-tricarbonyl labeled agents for cell labeling: Development, biodistribution in normal mice and preliminary in vitro evaluation. Bioorganic and Medicinal Chemistry, 2010, 18, 396-402.	3.0	7
151	Micro-HCCs in rats with liver cirrhosis: paradoxical targeting effects with vascular disrupting agent CA4P. Oncotarget, 2017, 8, 55204-55215.	1.8	7
152	Intra-individual comparison of therapeutic responses to vascular disrupting agent CA4P between rodent primary and secondary liver cancers. World Journal of Gastroenterology, 2018, 24, 2710-2721.	3.3	7
153	Metabolism of nitrogen-13 labelled ammonia in different conditions in dogs, human volunteers and transplant patients. European Journal of Nuclear Medicine and Molecular Imaging, 1995, 22, 116-121.	2.1	6
154	Photo isomerization of cis yclooctene to trans yclooctene: Integration of a microâ€flow reactor and separation by specific adsorption. AICHE Journal, 2021, 67, e17067.	3.6	6
155	Synthesis of 1-[18F]fluorodeoxyglucose: an unexpected rearrangement in the reaction of 2-O-methanesulfonyl-β-D-mannopyranose with [18f] fluoride. Journal of Labelled Compounds and Radiopharmaceuticals, 1999, 42, 147-157.	1.0	5
156	Molecular imaging of norepinephrine transporter-expressing tumors: current status and future prospects. Quarterly Journal of Nuclear Medicine and Molecular Imaging, 2020, 64, 234-249.	0.7	5
157	A nonsurgical porcine model of left ventricular dysfunction. Validation of myocardial viability using dobutamine stress echocardiography and positron emission tomography. International Journal of Cardiovascular Interventions, 2000, 3, 111-120.	0.5	4
158	Synthetic Pept-Ins as a Generic Amyloid-Like Aggregation-Based Platform for In Vivo PET Imaging of Intracellular Targets. Bioconjugate Chemistry, 2021, 32, 2052-2064.	3.6	4
159	Preclinical Evaluation of [¹¹ C]YC-72-AB85 for <i>In Vivo</i> Visualization of Heat Shock Protein 90 in Brain and Cancer with Positron Emission Tomography. ACS Chemical Neuroscience, 2021, 12, 3915-3927.	3.5	4
160	Synthetic strategies for radioligands for <i>in vivo</i> imaging of brain cannabinoid typeâ€l receptors. Journal of Labelled Compounds and Radiopharmaceuticals, 2013, 56, 207-214.	1.0	3
161	ICâ€Pâ€150: [Câ€11]MKâ€6884 PET: CHARACTERIZING BRAIN M4 RECEPTORS IN HEALTHY ELDERLY VOLUNTEE ACETYLCHOLINESTERASE INHIBITORSâ€TREATED AD PATIENTS. Alzheimer's and Dementia, 2019, 15, P121.	RS AND	3
162	Preclinical evaluation of [18F]cabozantinib as a PET imaging agent in a prostate cancer mouse model. Nuclear Medicine and Biology, 2021, 93, 74-80.	0.6	3

#	Article	IF	CITATIONS
163	[P3–316]: PRE LINICAL CHARACTERIZATION OF THE NOVEL TAU PET LIGAND [18F]â€JNJ'067. Alzheimer's ar Dementia, 2017, 13, P1069.	nd 0.8	2
164	Highlight selection of radiochemistry and radiopharmacy developments by editorial board. EJNMMI Radiopharmacy and Chemistry, 2021, 6, 13.	3.9	1
165	PET Imaging of Phosphodiesterases in Brain. , 2021, , 851-877.		1
166	Myocardial viability and Tc99m-MIBI: Correlation with PET, function and histology. Journal of the American College of Cardiology, 1996, 27, 162.	2.8	0
167	O2-10-03: In vivo characterization of basal forebrain atrophy and cholinergic denervation in primary progressive aphasia. , 2015, 11, P198-P198.		0